Received: 26 July 2019 | Accepted: 5 January 2020

DOI: 10.1002/mrd.23317

Molecular Reproduction & Development

RESEARCH ARTICLE

High-resolution imaging of the actin cytoskeleton and epithelial sodium channel, CFTR, and aquaporin-9 localization in the vas deferens

Sachin Sharma | Girishkumar K. Kumaran | Israel Hanukoglu

Laboratory of Cell Biology, Ariel University, Ariel, Israel

Correspondence
Israel Hanukoglu, Laboratory of Cell Biology, Ariel University, 40700 Ariel, Israel.
Email: mbiochem@gmail.com

Funding information
Ariel University Research and Development funds

Abstract

Vas deferens is a conduit for sperm and fluid from the epididymis to the urethra. The duct is surrounded by a thick smooth muscle layer. To map the actin cytoskeleton of the duct and its epithelium, we reacted sections of the proximal and distal regions with fluorescent phalloidin. Confocal microscopic imaging showed that the cylinder-shaped epithelium of the proximal region has a thick apical border of actin filaments that form microvilli. The epithelium of the distal region is covered with tall stereocilia (13–18 μm) that extend from the apical border into the lumen. In both regions, the lateral and basal cell borders showed a thin lining of actin cytoskeleton. The vas deferens epithelium contains various channels to regulate the fluid composition in the lumen. We mapped the localization of the epithelial sodium channel (ENaC), aquaporin-9 (AQP9), and cystic fibrosis transmembrane conductance regulator (CFTR) in the rat and mouse vas deferens. ENaC and AQP9 immunofluorescence were localized on the luminal surface and stereocilia and also in the basal and smooth muscle layers. CFTR immunofluorescence appeared only on the luminal surface and in smooth muscle layers. The localization of all three channels on the apical surface of the columnar epithelial cells provides clear evidence that these channels are involved concurrently in the regulation of fluid and electrolyte balance in the lumen of the vas deferens. ENaC allows the flow of Na^+ ions from the lumen into the cytoplasm, and the osmotic gradient generated provides the driving force for the passive flow of water through AQP channels.

KEYWORDS
ductus deferens, reproductive tract, smooth muscle, stereocilia

1 | INTRODUCTION

In mammals, spermatozoa are produced in the seminiferous tubules and flow into the epididymal duct. The end of the epididymis is connected to the vas deferens (also known as ductus deferens). In rats, the vas deferens is ~5 cm long and in humans ~30 cm long. The vas deferens ends with an opening into the ejaculatory duct at a point where the duct of the seminal vesicle also joins the ejaculatory duct (Treuting, Dintzis, & Montine, 2017).

The vas deferens duct is surrounded by a thick smooth muscle layer that is composed of three layers: A thick middle circular layer in between an inner and an outer longitudinal smooth muscle layers. This muscle layer is bounded by adventitia that is the outermost connective tissue (Treuting et al., 2017). The smooth muscle layers surrounding the vas deferens duct are innervated mostly by

adrenergic nerves. The activation of these nerves initiates the peristaltic contraction and relaxation of the smooth muscle layers, ejecting the sperm population down the vas deferens and into the urethra (Koslov & Andersson, 2013).

The initial (proximal) segment of the vas deferens is characterized by a cylindrical lumen. Towards the middle of the duct, the epithelium becomes crenulated, marking the beginning of the distal region of the vas deferens. From the beginning to the end, the vas deferens epithelium is lined by columnar epithelial cells called principal cells (Hamilton & Cooper, 1978; Hoffer, 1976).

The vas deferens epithelium plays a significant role in the maintenance of the luminal environment necessary for the maturation of sperm (Da Silva, Piétrement, Brown, & Breton, 2006; Hinton & Palladino, 1995; Wong, Gong, Leung, & Cheuk, 2002). Along the long route extending from the seminiferous tubules, via rete testis, epididymis caput, and cauda segments, the values of major biochemical parameters such as pH, concentration of ions, osmolarity, and protein composition of the luminal fluid show significant differences (Clulow, Jones, & Hansen, 1994; Cooper & Yeung, 2003; Dacheux & Dacheux, 2014; Johnson & Howards, 1977; Levine & Kelly, 1978; Zhou, De Iuliis, Dun, & Nixon, 2018). The common trend is a decrease in the pH (acidification down to pH 6.64–6.85, in the rat; and 5.8, in the bull cauda epididymis; Carr, Usselman, & Acott, 1985; Levine & Kelly, 1978; Levine & Marsh, 1971), and an increase in the sperm concentration (spermatocrit; Howards, Jessee, & Johnson, 1975; Jindal, 1984; Jones, 1980; Levine & Marsh, 1971) towards the distal end of the epididymis. At low pH, the sperm remain in a quiescent state in the cauda, and increasing the pH to 7.5 enhances the motility of the sperm (Acott & Carr, 1984). An interesting study showed that the pH of the vas deferens luminal fluid is increased up to pH 7.5 by the addition of an alpha-adrenergic agonist (Pierucci-Alves, Duncan, Lillich, & Schultz, 2010). Thus, adrenergic stimulation not only ejects the sperm but also initiates luminal fluid changes that promote sperm maturation and motility.

The processes of fluid absorption, regulation of electrolyte, and proton concentrations are dependent on the function of many ion and water channels and various transporters on both the apical and the basolateral borders of epithelial cells. Of these, the family of aquaporin (AQP) water channels that includes 13 isoforms has been most extensively studied as these channels are involved in water absorption that leads to the concentration of the luminal fluid. Twelve of the AQP isoforms are expressed in the male and female reproductive systems (Yeste, Morató, Rodríguez-Gil, Bonet, & Prieto-Martínez, 2017; Zhang, Tan, Qu, Sheng, & Huang, 2012). Specifically, the expressions of AQP1, AQP2, AQP7, and AQP9 have been documented in the vas deferens of several species (Andonian & Hermo, 1999; Khadijah Ramli, Giribabu, Karim, & Salleh, 2019; Pastor-Soler et al., 2001; Rojek et al., 2007; Schimming, Pinheiro, de Matteis, Machado, & Domeniconi, 2015; Yeste et al., 2017).

Since AQPs are passive channels, the flow of water from the lumen into the cells via AQPs is dependent on an osmotic gradient. Sodium ions are the major determinants of luminal fluid osmolarity because, among the electrolytes, their concentration is the highest (Clulow, Jones, Hansen, & Man, 1998; Jenkins, Lechene, & Howards, 1980; Levine & Marsh, 1971). Extensive evidence for the involvement of epithelial sodium channel (ENaC) in the transcellular flow of Na^+ was provided by Carlin, Lee, Marcus, and Schultz (2003) who showed that ion transport across epithelial cells derived from porcine and human vas deferens is inhibited by amiloride—an inhibitor of ENaC (Phillips & Schultz, 2002). In addition, they provided evidence for the expression of the messenger RNA (mRNAs) of all three ENaC subunits in porcine vas deferens epithelia (Carlin et al., 2006). These studies indicated that ENaC plays a role in generating the osmotic gradient that drives the transcellular flow of water through AQP channels (Figure 1).

Cystic fibrosis transmembrane conductance regulator (CFTR) is another ion transporter that is expressed in the vas deferens and modulates the composition of the luminal fluid in the male reproductive tract (Bertog et al., 2000; Carlin et al., 2006; Cheung, Leung, Leung, & Wong, 2003; Khadijah Ramli, Giribabu, & Salleh, 2018; Reynaert et al., 2000). CFTR is a cAMP activated anion channel that secretes mainly Cl^- ions, and to a lesser extent, HCO_3^- (Csanády, Vergani, & Gadsby, 2019; Saint-Criq & Gray, 2017). By secreting bicarbonate ions, CFTR also plays a role in modulating the pH of the luminal fluid.

The most common male infertility disorder associated with vas deferens is the congenital absence of the vas deferens accounting for obstructive azoospermia. In a systematic review and meta-analysis, 78% of the patients with congenital bilateral absence of the vas deferens were found to have at least one CFTR mutation (Chen, Ruan, Xu, Chen, & Chan, 2012; de Souza, Faucz, Pereira-Ferrari, Sotomaior, & Raskin, 2018; Yu, Chen, Ni, & Li, 2012). Among patients with congenital unilateral absence of the vas deferens (CUAVD), 46% had at least one CFTR variant (Cai et al., 2019). Schlegel, Shin, and Goldstein (1996) reported that 26% of patients with CUAVD also suffer from ipsilateral renal agenesis. The majority of male patients (9,798%) affected by cystic fibrosis (CF) due to mutations in the

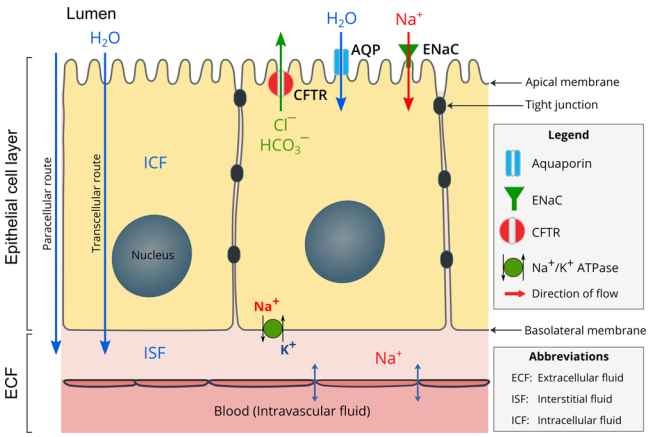

FIGURE 1 Diagram showing the location and function of water and ion channels on the vas deferens epithelia examined in this study. Both aquaporin and ENaC are localized on the apical membrane and the microvilli and stereocilia on the apical surface. CFTR is localized on the apical membrane but does not appear on stereocilia. AQP, aquaporin; CFTR, cystic fibrosis transmembrane conductance regulator; ENaC, epithelial sodium channel

CFTR gene are nearly infertile (Chen et al., 2012; Osborne et al., 1993). A CFTR gene-knockout rat with $CFTR^{-/-}$ genotype also exhibited a bilateral absence of the vas deferens and a phenotype that resembled features observed in CF (Tuggle et al., 2014).

Several approaches have shown that CFTR may influence the functions of both AQP and ENaC.

These include studies coexpressing CFTR in Xenopus oocytes together with an AQP isoform (Cheung et al., 2003 Gentzsch et al., 2010) or ENaC subunits (Rauh, Hoerner, & Korbmacher, 2017), analysis of the effects of CFTR mutations on ENaC activity in patients with CF (Althaus, 2013), simulations of ENaC–CFTR interactions (Horisberger, 2003), and transgenic mouse models overexpressing ENaC (Zhou-Suckow, Duerr, Hagner, Agrawal, & Mall, 2017). The validity of some of the earlier studies showing inhibition of ENaC by CFTR in Xenopus oocytes has been critically evaluated (Nagel et al., 2005). However, the mechanism(s) of CFTR influence on ENaC function has not been clearly established. The hypotheses raised so far include direct interaction between CFTR and ENaC, the effect of CFTR on ENaC expression/activation, and electrical coupling.

We first examined the expression of ENaC in the female reproductive tract following the report that a pseudohypoaldosteronism (PHA) patient with a nonsense mutation in the SCNN1A gene coding for the alpha ENaC subunit (ENaCA) had fertility problems (Enuka, Hanukoglu, Edelheit, Vaknine, & Hanukoglu, 2012). For this purpose, we generated polyclonal antisera against ENaCA, and using these antisera, we showed that in multiciliated cells in the respiratory airways and the female reproductive tract, ENaC is localized on the cell membrane covering the entire length of motile cilia (Enuka et al., 2012), while CFTR is localized on the apical membrane but not on cilia (Enuka et al., 2012; Kreda & Gentzsch, 2011).

ENaC is a channel that is composed of three subunits (Hanukoglu, 2017; Hanukoglu & Hanukoglu, 2016). In earlier studies, we showed that the assembly of a full heterotrimer of ENaC depends on three intact subunits and even missense mutations in a single subunit can inhibit cell-surface localization of ENaC (Edelheit, Ben-Shahar, Dascal, Hanukoglu, & Hanukoglu, 2014; Edelheit et al., 2010; Hanukoglu et al., 2008). As expected by these findings, we observed that ENaC expression could hardly be detected in the endometrial biopsy samples from the PHA patient with the nonsense mutation in ENaCA (Boggula, Hanukoglu, Sagiv, Enuka, & Hanukoglu, 2018).

As our studies revealed that ENaC is expressed in the female reproductive tract and is essential for fertility, we then proceeded to examine ENaC localization in the male reproductive tract. By using confocal microscopy, we showed that both ENaC and CFTR are expressed in the male reproductive tract epithelia, including the seminiferous tubules and the epididymis but with major differences in their cellular and subcellular localizations (Sharma & Hanukoglu, 2019; Sharma, Hanukoglu, & Hanukoglu, 2018).

We undertook the present study, to map the sites of localization of AQP, ENaC, and CFTR in the vas deferens. Recently, the expression of the gamma subunit of ENaC was shown at a low resolution in a partial section of a distal segment of the rat vas deferens by immunohistochemistry (Khadijah Ramli et al., 2018). We aimed to answer the following questions: Is ENaC expressed in both proximal and distal segments of the vas deferens? Is ENaC expressed in all principal cells or a subpopulation? Is ENaC localized in the cytoplasm (as we had described in our earlier study on the seminiferous tubules) or is it localized on the cell membrane? Is ENaC localized on the stereocilia that cover the surface of the principal cells? Is ENaC expressed in the smooth muscle cells that surround the vas deferens epithelia? In addition to these questions, we examined the localization of the AQP and CFTR in view of their effects on ENaC activity mentioned above.

Histological studies have shown that the apical borders of the epithelial cells in the vas deferens are covered by microvilli or stereocilia (Francavilla et al., 1987; Hamilton & Cooper, 1978; Höfer & Drenckhahn, 1996; Rodriguez & Bustos-Obregón, 1993). Both microvilli and stereocilia are cell projections that have backbones composed of actin filament bundles (Pelaseyed & Bretscher, 2018). In epithelial cells, a network of actin filaments lies underneath the membrane providing structural support for the membrane. This network called the actin cortex or cortical actin cytoskeleton is a dynamic structure (Clausen, Colin-York, Schneider, Eggeling, & Fritzsche, 2017; Doctor, 2006). Actin filaments may be linked to membrane proteins directly or with other intermediary proteins (Sasaki, Yui, & Noda, 2014).

In our studies on the mapping of ion channels in epithelial tissues, we have established the principle to verify the integrity of the cytoskeletal structure of tissues as an essential step in mapping channel localization (Enuka et al., 2012; Hanukoglu et al., 2017; Sharma et al., 2018). We recently also showed that the actin cytoskeletal structure allows the identification and classification of epithelial cells in the kidney (Kumaran & Hanukoglu, 2020). Thus, in this study, for the first time, we visualized the actin cytoskeleton of the proximal and distal regions of the vas deferens epithelia using phalloidin that binds to actin filaments. Our results revealed that both ENaC and AQP9 are localized on the apical border of the epithelia and on stereocilia. These results provide evidence for the regulation of luminal osmolarity by ENaC, allowing the transcellular flow of water via AQP9 to lead to concentration of the sperm in the vas deferens (Figure 1).

2 | RESULTS

2.1 | Actin cytoskeleton

Previous studies on the histology of the vas deferens showed that the epithelium that covers the proximal region is in a cylindrical shape; whereas the epithelium in the distal region has large folds that protrude into the lumen similar to the folds of a drape (Hamilton & Cooper, 1978). The actin cytoskeleton that phalloidin fluorescence revealed in the rat vas deferens matched this morphology on the apical border of the epithelium of both regions: A nearly perfect cylindrical shape on the apical border of the proximal region (Figure 2), and drape-like large folds in the distal region (Figure 3).

Images of the proximal and the distal regions revealed the following similarities and differences in the actin cytoskeleton of the epithelial cells

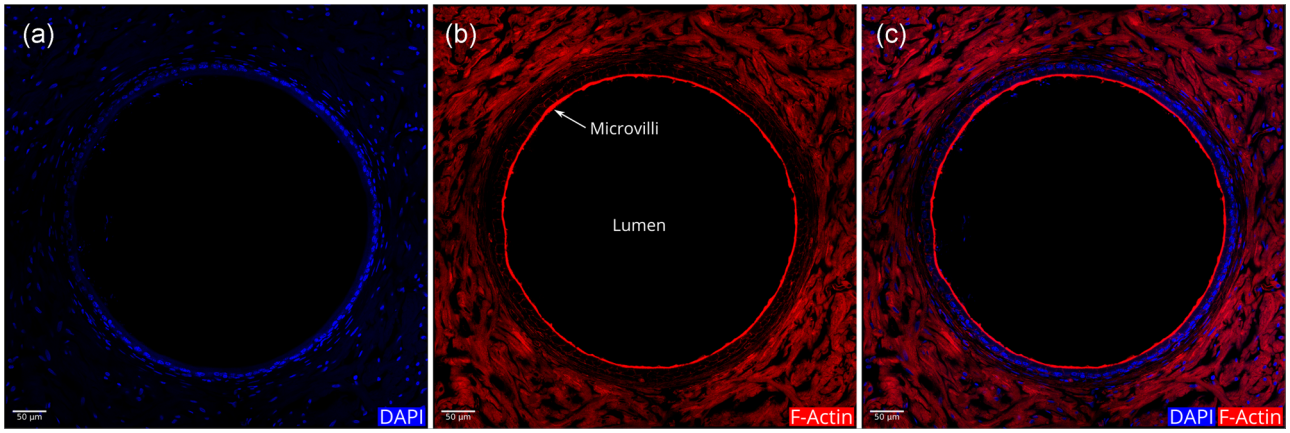

FIGURE 2 Distribution of actin filaments in a cross-section of the proximal region of rat vas deferens. (a) Blue DAPI staining that marks the cell nuclei. (b) Red phalloidin that stains the actin filaments. (c) Merged image of (a) and (b). The strong actin fluorescence of the luminal border reflects the presence of short microvilli. A thin line of actin cytoskeleton demarcates the lateral and the basal borders of the epithelial cells. The thick staining of actin filaments surrounding the inner mucosa of the vas deferens marks the smooth muscle layers. The diameter of the proximal duct shown here is ~430 µm

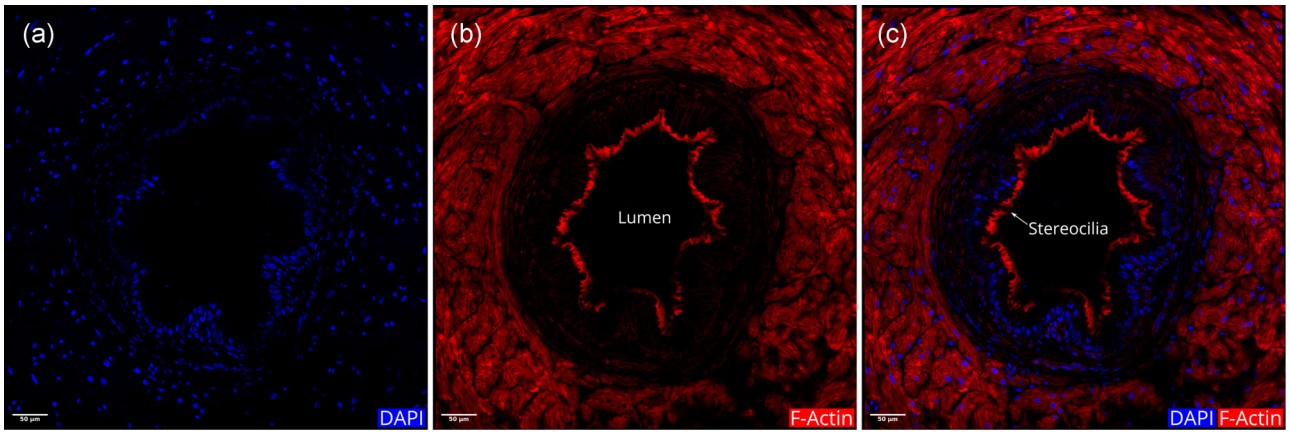

FIGURE 3 Distribution of actin filaments in a cross-section of the distal region of the rat vas deferens. (a) Blue DAPI staining that marks the cell nuclei. (b) Red phalloidin that stains the actin filaments. (c) Merged image of (a) and (b). The luminal border of the single columnar epithelium shows a wavy pattern of phalloidin staining. The border along the length of each cell in the columnar epithelium is also marked by red-colored phalloidin fluorescence. The thick staining of actin filaments surrounding the inner mucosa of the vas deferens marks the smooth muscle layers

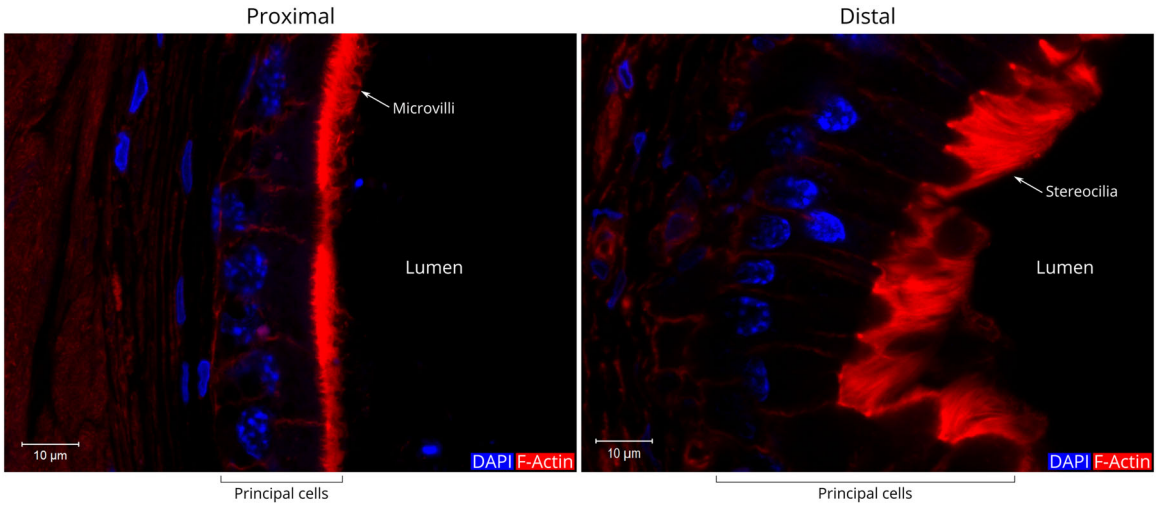

FIGURE 4 Magnified views of the proximal and distal regions of the rat vas deferens. The average height of the principal cells (without the microvilli or stereocilia) is 16.8 µm in the proximal region; and 36.6 µm in the distal region. While the height of the microvilli in the proximal region is 2–5 µm, and the height of the stereocilia is in the range of 13–18 µm. In the distal region, individual fibers of stereocilia are visible within tufts of stereocilia, and that each bundle of fibers is associated with a single cell of columnar epithelium

(Figure 4): In both regions, the actin cytoskeleton appears as a thin lining along the lateral and basal borders of the principal cells. In contrast, the apical borders of the principal cells have a thick fuzzy lining of actin filaments. In the proximal region, the apical actin filaments form microvilli that have a height of 2–5 μm (Figure 4), similar to that previously reported (Kennedy and Heidger, 1979). In the distal region, the apical actin filaments form long stereocilia that are much taller (13–18 μm; Figure 4). In the distal region, individual fibers of stereocilia are visible within tufts, and each bundle of fibers is clearly associated with a single cell of the columnar epithelium (Figure 4).

In both regions, the cytoplasmic space of the epithelial cells was nearly devoid of phalloidin fluorescence (Figure 4). In contrast, the cytoplasm of the smooth muscle cell layers surrounding the epithelium showed almost uniform phalloidin fluorescence with a pattern typical of smooth muscle cells (Figures 2 and 3).

A cross section of the distal vas deferens of a mouse showed a distribution of actin filaments similar to that observed in the rat distal vas deferens (Figure 5). In a magnified view of the principal cells, a thin actin bundle is seen along the lateral border of each cell (Figure 5e,f). In contrast, the apical border of each cell is covered with a thick tuft of stereocilia (Figure 5e,f).

2.2 | ENaC localization

To visualize the localization of ENaC, we used a previously described polyclonal antibody. To confirm the specificity of this antiserum for use in the vas deferens, we reacted a blot containing total tissue protein from rat lung, vas deferens, epididymis, and testis samples with anti-ENaCα antisera (Figure 6). As expected, the major ENaCα subunit band appeared at ~75 kDa in all tissue samples. In the vas deferens samples, we observed two additional bands at ~90 kDa and above 100 kDa (Figure 6). The ~90-kDa band may be the result of hyperglycosylation in the α-subunit of ENaC (Canessa, Merillat, & Rossier, 1994; Hanukoglu et al., 2017; Snyder, McDonald, Stokes, & Welsh, 1994). The higher molecular weight band has been observed in other studies using different antibodies (Hughey et al., 2003). This may be the product of alternative processing of the mRNA encoded by the SCNN1A gene

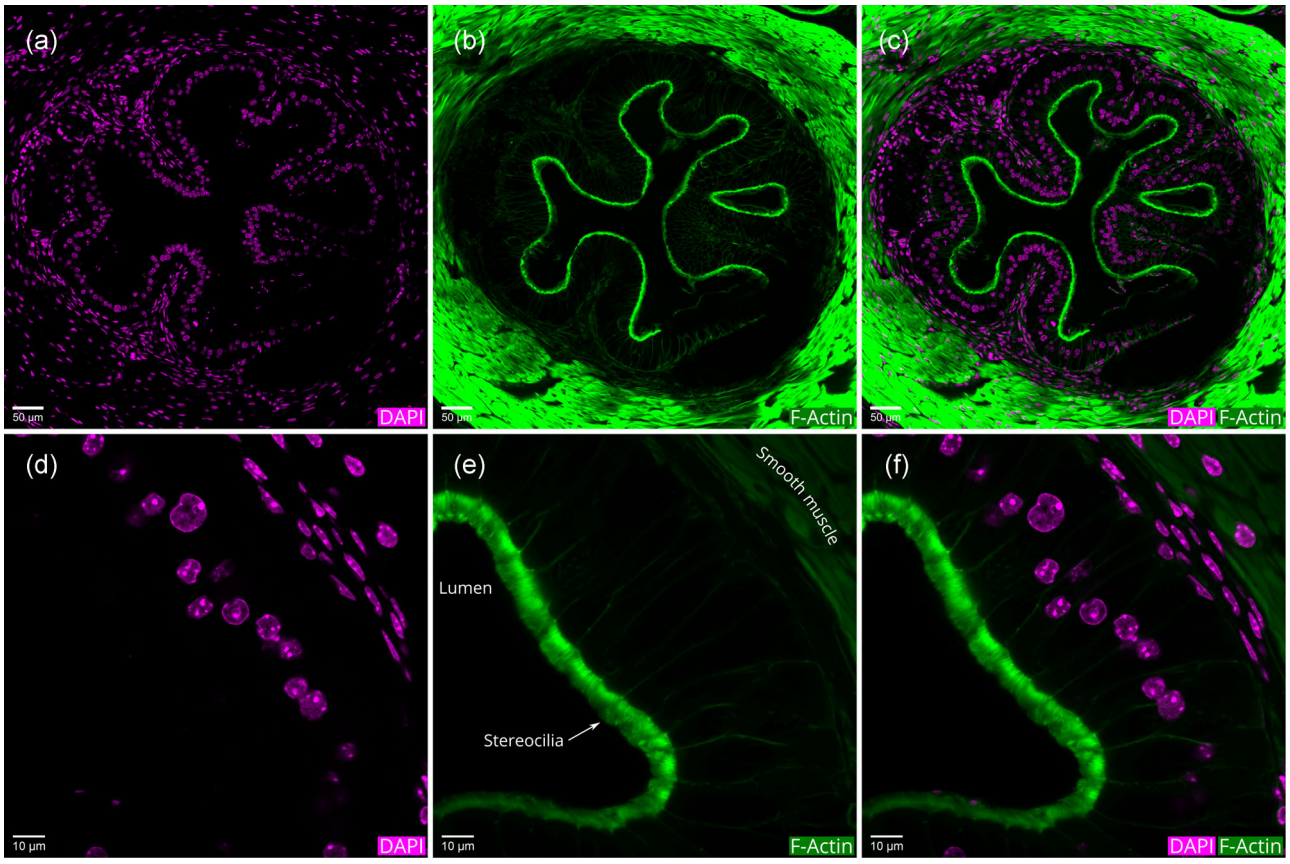

FIGURE 5 Distribution of actin filaments in a cross-section of the mouse vas deferens. The section was reacted with green phalloidin that binds to the actin filaments and DAPI that stains the cell nuclei (magenta colored). (a) DAPI fluorescence; (b) F-actin fluorescence; (c) merged image of (a) and (b). The thick staining of actin filaments surrounding the inner mucosa of the vas deferens marks the smooth muscle layers. (d–f) A magnified view of the principal cells. (d) DAPI fluorescence; (e) F-actin fluorescence; and (f) merged image of (d) and (e). A thin bundle of actin filaments appears at the lateral border of each cell, and a thick tuft of stereocilia is located on the apical border of each cell facing the lumen. The mean height of the principal cells was 54.9 ± 3.4 μm, and the mean height of the stereocilia was 8.1 ± 0.5 μm. The variance shown is the standard deviation

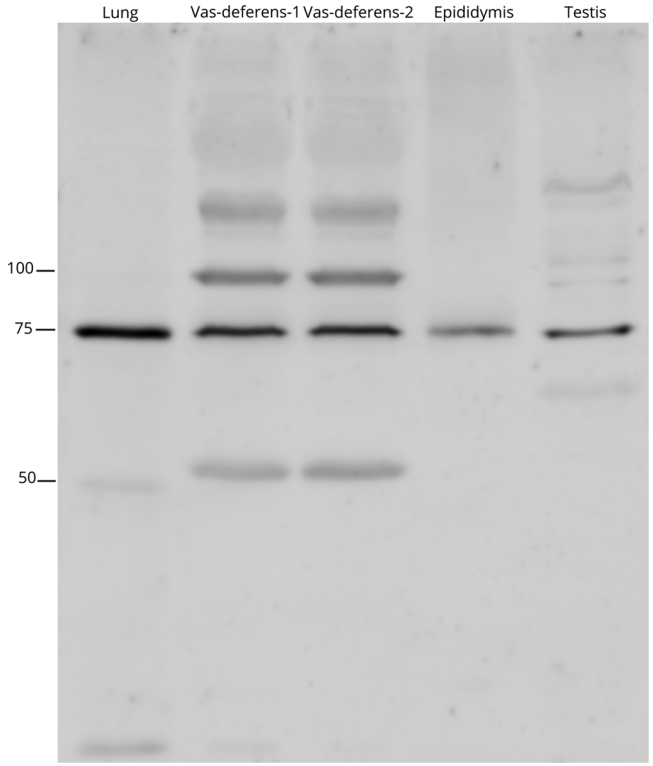

FIGURE 6 Western blot analysis of the rat lung, vas deferens, epididymis, and testis tissue lysate samples. The blot was reacted with anti-ENaCα antisera. Lung, epididymis, and testis lanes were loaded with 75-μg total tissue protein. The two vas deferens lanes (1 and 2) were each loaded with 50-μg total tissue protein isolated from two different animals. ENaCα, epithelial Na^+ channel α-subunit

(Thomas, Auerbach, Stokes, & Volk, 1998). ENaCα subunit has been observed to undergo specific proteolytic processing to yield two fragments of ~50 and ~25 kDa (Enuka et al., 2012; Hughey et al., 2003). While in the epididymis and testis, we could hardly detect a proteolytic processing product, in the vas deferens, there was a prominent ~50-kDa fragment, that is, most likely a proteolytic processing product.

The reaction of anti-ENaCα with sections of the proximal region of the rat vas deferens revealed the strongest fluorescence on the apical border of the principal cells (Figure 7). In the distal region, anti-ENaCα immunofluorescence was observed on the apical border of the principal cells, in the cytoplasm of the basal cells, and in the smooth muscle layers (Figure 7).

In Figures 7 and 8, DAPI-stained nuclei of the principal cells can be easily distinguished by their large size, oval shape, and dense intranuclear granules. These special features were also visualized by electron microscopy of human vas deferens (Hoffer, 1976). In both proximal and distal regions, the cytoplasmic space between the principal cell nuclei and the apical membrane was completely devoid of ENaC immunofluorescence (Figures 7 and 8). In a whole section of the distal region, we could identify only 2–3 principal cells, wherein ENaC immunofluorescence appeared between the nuclei and the apical membrane.

The anti-ENaCα immunofluorescence starts at the apical membrane and extends into the lumen (Figure 8). Yet, the length of the red ENaC immunofluorescence starting at the apical border and extending into the lumen (Figure 8) appeared longer than the length of the stereocilia shown in Figure 5. The principal cells in the mid-region of both rat and human vas deferens have apocrine secretions resulting from the blebbing of the apical surface into the lumen (Andonian & Hermo, 1999; Andonian, Jarvi, Zini, & Hermo, 2002). Therefore, most likely some of the ENaC immunofluorescences seen in the lumen represent ENaC in blebs detached from the cell surface.

The second type of cell in the vas deferens epithelia is small basal cells that that are located between the row of principal cells and the

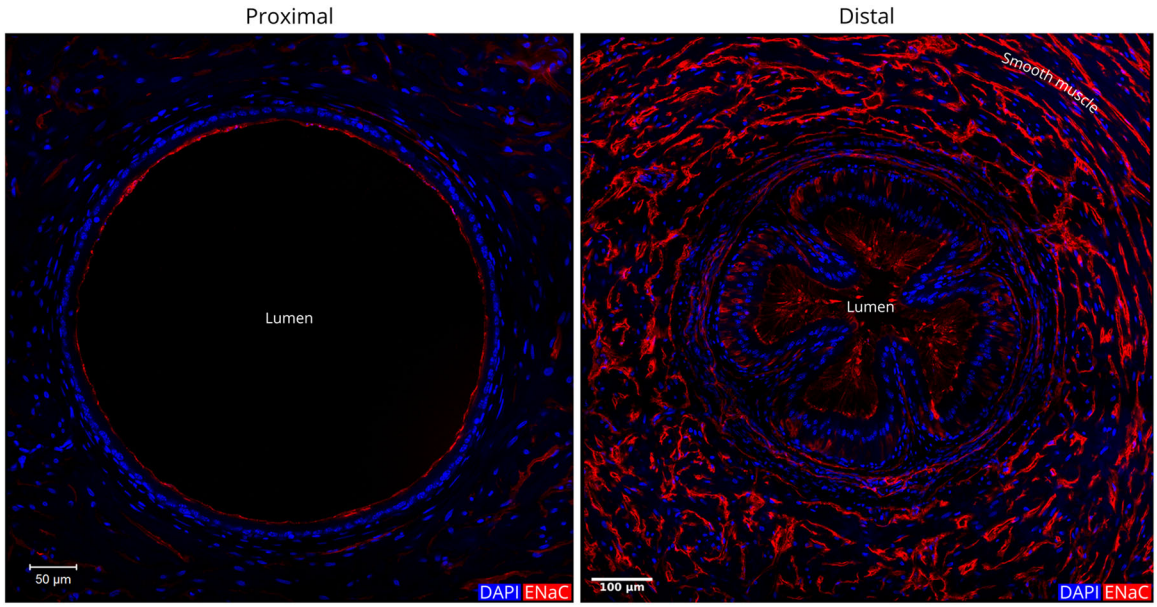

FIGURE 7 Images of the cross sections of the proximal and distal parts of the rat vas deferens reacted with anti-ENaCα antisera. These images were generated by tile scanning: 2 × 2 for the proximal region and 3 × 3 for the distal region of the rat vas deferens. The red-colored ENaC immunofluorescence appeared along the luminal border and the tufts of stereocilia projecting into the lumen. ENaC immunofluorescence also appeared in the smooth muscle layers of the vas deferens

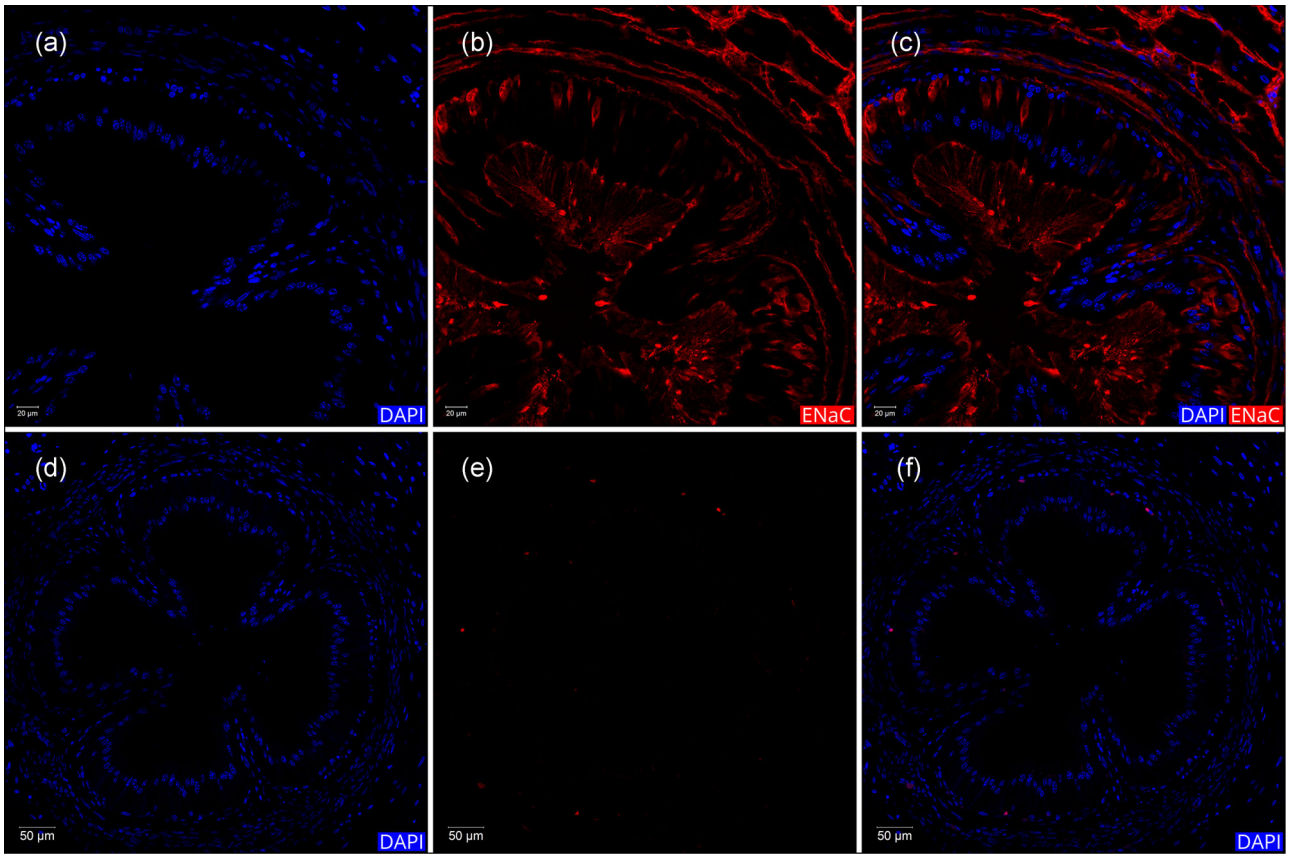

FIGURE 8 A magnified view of the inner mucosa of the rat vas deferens reacted with anti-ENaCα antisera (upper row, (a–c). The lower row (d–f) shows fluorescence in a section reacted with DAPI and secondary antisera alone. (a and d) DAPI staining of the cell nuclei. (b) Anti-ENaCα antisera immunofluorescence. (e) Control slide without primary antisera. (c and f) Merged images. ENaC immunofluorescence appears clearly on the luminal surface and along the stereocilia protruding into the lumen. Note that the cytoplasm of columnar epithelium cells showed hardly any ENaC immunofluorescence. Yet, there were scattered cases of cytoplasmic staining close to the basal layer

basement membrane (Hoffer, 1976). The DAPI-stained nuclei of the basal cells are clearly distinguishable by their small size, and distance from the principal cell nuclei (Figures 7 and 8). The cytoplasmic region surrounding the nuclei of the basal cells was also without any detectable ENaC immunofluorescence (Figures 7 and 8). Yet, in some principal cells, between the principal cell nuclei and the basal cell nuclei, there appeared ENaC immunofluorescence (Figure 8). The stromal cells beneath the columnar epithelium also showed strong anti-ENaCα immunofluorescence (Figure 8b).

The lower row of Figure 8 shows a control slide that was reacted only with the secondary antiserum without the primary antiserum (Figure 8e). In this control slide, only DAPI fluorescence was observed (Figure 8f).

To confirm ENaC localization on stereocilia, we reacted to a section of a mouse distal vas deferens with both phalloidin and anti-ENaCA. In a magnified image, it can be seen clearly that anti-ENaCA immunofluorescence is specifically localized on the stereocilia that cover the apical surface of the principal cells (Figure 9, top row). Magnifying this image further it can be seen that ENaC immunofluorescence is observed as dots on the cell surface (Figure 9b). In this distal section, we could not see signs of blebbing as seen in the rat vas deferens section (Figure 8). This is not surprising as apical blebbing is observed in the middle of vas deferens (Andonian & Hermo, 1999).

A study that examined the localization of the ENaCγ (ENaCG) subunit by immunohistochemistry showed staining nearly in the entire row of rat epithelial cells including the cytoplasm (Khadijah Ramli et al., 2018). The authors noted that ENaC is also located on the basolateral membrane. This study further showed that ENaCG expression can be enhanced by testosterone treatment. In this study, we observed ENaC immunofluorescence on the apical surface of the principal cells of the epithelia and hardly any in the cytoplasm (with the exceptions noted above). In contrast to the results of Khadijah Ramli et al., we did not observe any ENaC immunofluorescence on the basolateral membrane of the principal cells or in the row of basal cells. The strong intracytoplasmic staining observed by Khadijah Ramli et al. may be a result of the induction of expression of ENaC genes by the testosterone treatment of the animals.

2.3 | AQP9 and CFTR localization

The localization of the water-selective channel AQP9 in the distal region of rat vas deferens was very similar to that of ENaC (Figure 10).

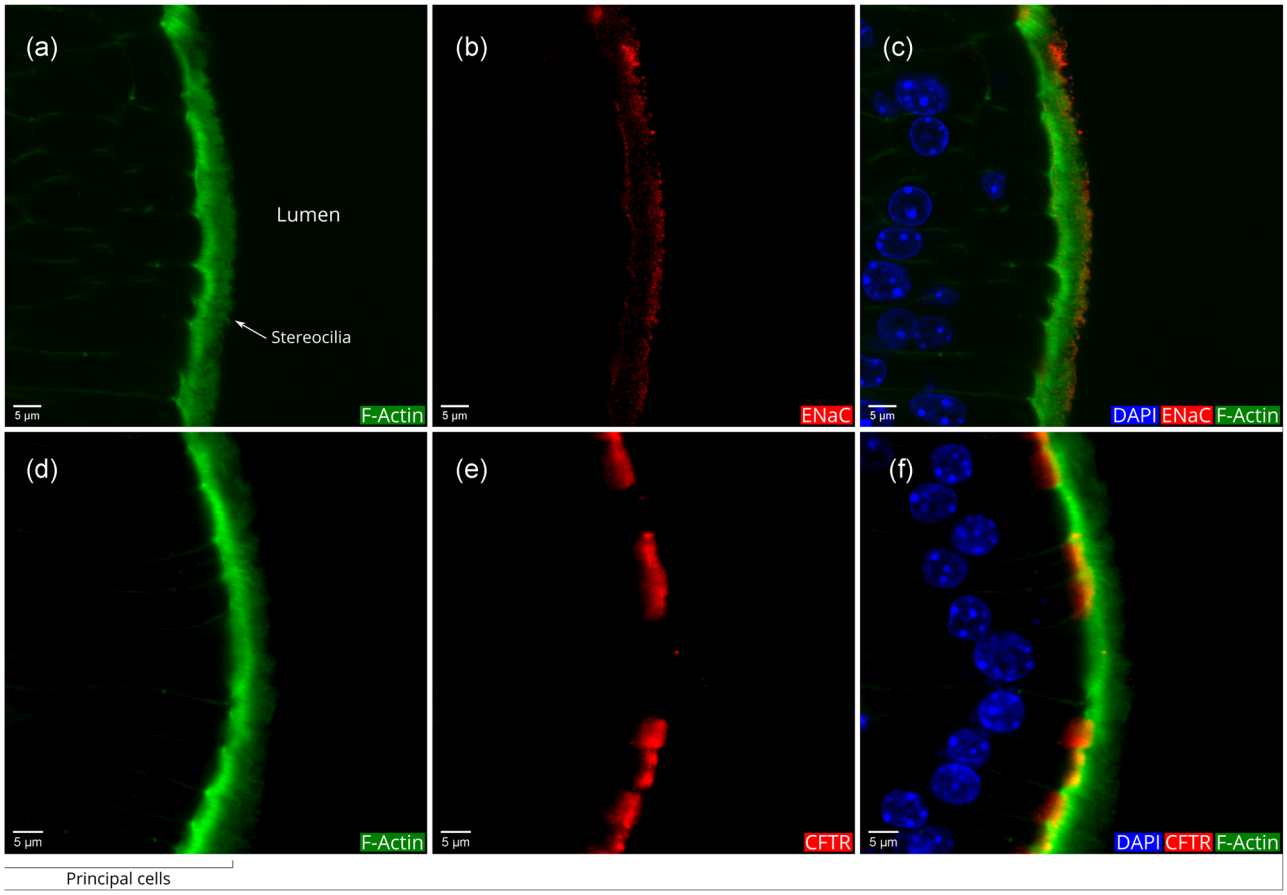

FIGURE 9 Localization of ENaC and CFTR in a mouse vas deferens section. (a) Phalloidin fluorescence of the actin filaments. (b) Anti-ENaCα immunofluorescence. (c) Merged image of (a) and (b) with DAPI fluorescence of nuclei. (d) Phalloidin fluorescence of the actin filaments, (e) anti-CFTR immunofluorescence, and (f) merged image of (d) and (e) with DAPI fluorescence. The sections were taken at ~5 mm from the end of the distal region of vas deferens

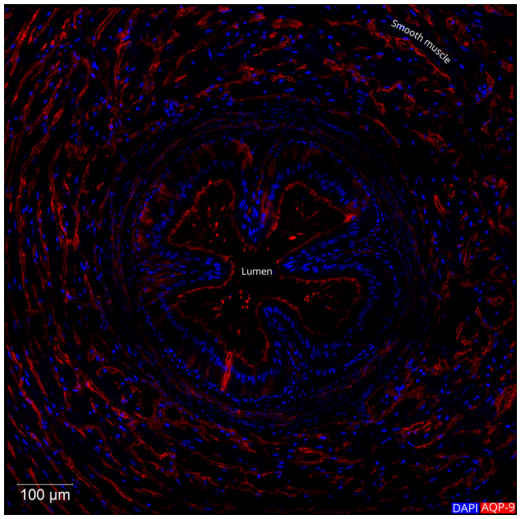

FIGURE 10 A tile-scan (3 × 3) image of a cross-section of the distal region of the rat vas deferens showing the localization of aquaporin-9 (AQP9) channel. The red-colored (AQP9) immunofluorescence appeared on the luminal surface of the epithelium and on the stereocilia projecting from the epithelium into the lumen of the duct

Specifically, the cytoplasm in the columnar epithelium was devoid of AQP9 immunofluorescence (Figure 10 and in magnified view Figure 11). AQP9 immunofluorescence appeared on the luminal surface of the vas deferens epithelium, on the basal cell layer, the stromal cells, and the smooth muscle layers (Figure 10). AQP9 immunofluorescence was also strong along the stereocilia in the lumen (Figure 11).

In a control experiment, wherein we preincubated anti-AQP9 antiserum with a control antigen before adding the mixture into the reaction, no significant AQP9 immunofluorescence was observed in the epithelium (Figure 11e). In such control slides, only blue-colored DAPI staining was visible (Figure 11f).

In contrast to ENaC and AQP9, CFTR immunofluorescence was primarily localized uniformly on the luminal surface of the rat vas deferens and no luminal staining on the stereocilial extensions was observed (Figure 12). The dispersed staining of CFTR also appeared in the smooth muscle layers (Figure 12). A control slide, wherein the anti-CFTR antiserum was preincubated with antigen peptide showed hardly any CFTR immunofluorescence (results not shown).

To confirm CFTR localization on the apical border of principal cells, we reacted to a section of mouse distal vas deferens with both phalloidin and anti-CFTR. In a magnified image, it can be seen clearly that

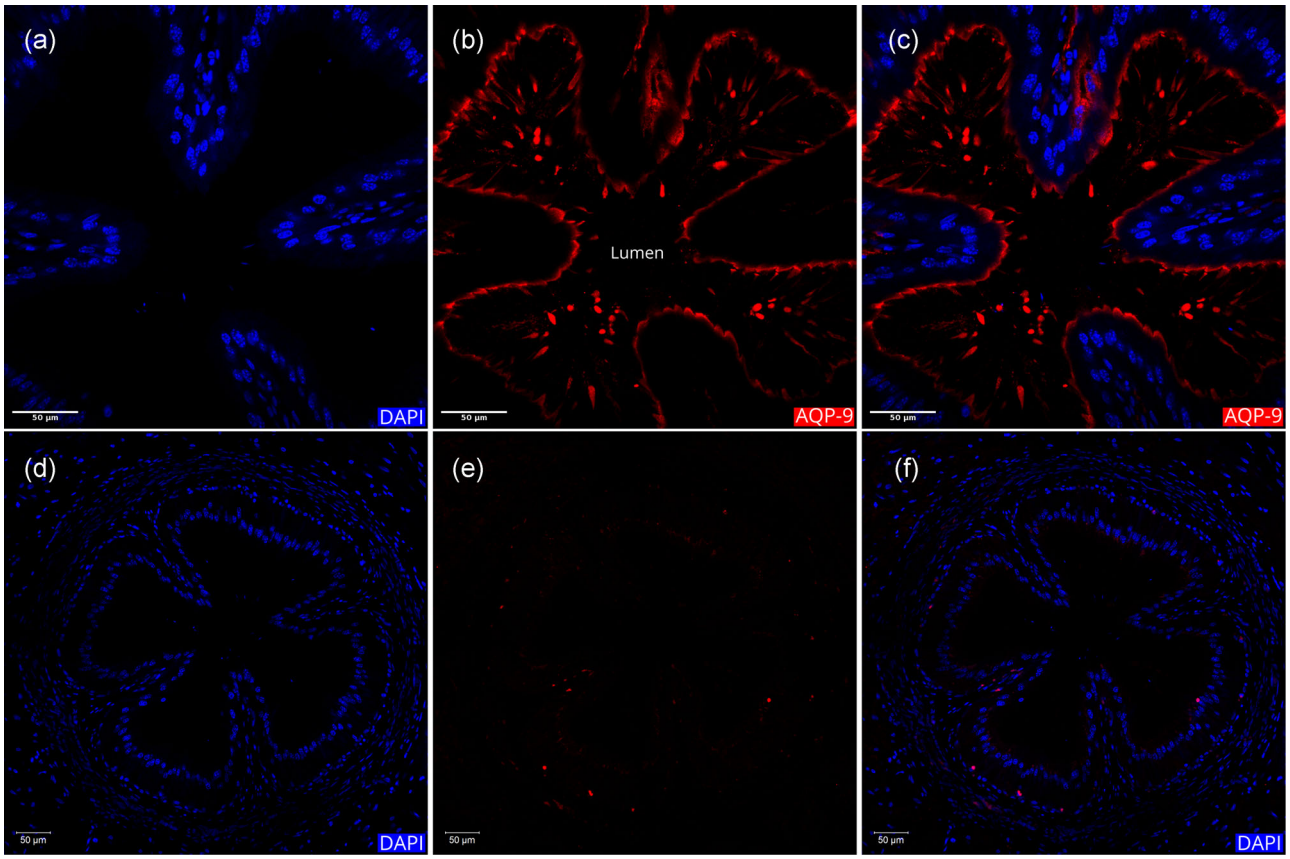

FIGURE 11 A magnified view of the inner mucosa of the distal region of a rat vas deferens. (a and d) DAPI staining of the cell nuclei. (b) Anti-AQP9 antisera immunofluorescence. (e) Control slide after anti-AQP9 antiserum was preincubated with control antigen peptide. (c and f) Merged images

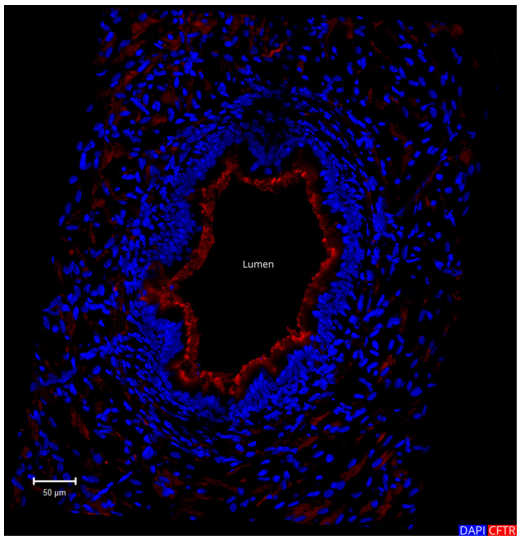

FIGURE 12 Visualization of CFTR localization in the distal region of rat vas deferens duct section reacted with anti-CFTR antisera. This three-dimensional image was generated from a z-stack of 16 optical slices (~1 µm/slice). CFTR immunofluorescence nearly uniformly covers the luminal surface of the columnar epithelium. CFTR immunofluorescence also appeared in a dispersed pattern in the smooth muscle cells that surround the inner mucosa

anti-CFTR immunofluorescence is specifically localized below the stereocilia that cover the apical surface of the principal cells (Figure 9, bottom row). Comparing the top row for ENaC and the bottom row for CFTR, it can be seen that while ENaC immunofluorescence appears on the stereocilia, CFTR immunofluorescence appears below the stereocilia (Figure 9, bottom row). It is also noteworthy that a few scattered cells in the row of columnar epithelia do not seem to have CFTR expression (Figure 9, bottom row). We had described a similar situation for CFTR expression in the cauda region of the rat epididymis (Sharma & Hanukoglu, 2019). The continuous actin-based fluorescence and the intact principal cell nuclei (as described above) provide evidence that there is no tear in the cell envelope (Figure 9d).

3 | DISCUSSION

3.1 | Actin cytoskeleton, microvilli, and stereocilia in the vas deferens epithelia

This study for the first time provided visualization of the actin cytoskeleton in whole sections of the epithelia in the proximal and distal regions of vas deferens by using fluorescent phalloidin that binds to actin filaments. Our results showed that in the rat vas

deferens proximal region, the apical border is uniformly covered with microvilli of 2–5 μm, and the distal region with much taller (13–18 μm) stereocilia (Figures 2 and 3). These microvilli and the stereocilia on the apical surface of the columnar epithelial cells increase greatly the surface area of each cell, allowing the localization of many more channels on the cell membrane.

Our high-resolution confocal microscopy images showed well preserved and complete images of stereocilia bundles of individual cells (Figures 4, 5, and 9). Previous studies on the histology of the vas deferens using either histochemical staining or electron microscopic ultrastructure showed mostly cut and scattered stereocilia, for example, Francavilla et al. (1987) and Khadijah Ramli et al. (2018, 2019) that do not represent the dense organization and the structure of the actin bundles.

Both the microvilli and the much longer stereocilia have backbones that are composed of bundles of actin filaments (Brown & McKnight, 2010; Pelaseyed & Bretscher, 2018). The actin filaments are tethered to the cell membrane by actin-binding proteins. The structure and function of stereocilia have been most extensively studied in the auditory epithelium of vertebrates (Fettiplace & Kim, 2014). Stereocilia in these epithelia have incremental heights and are arranged in a staircase configuration. In high-resolution images of the stereocilia in the distal region of the vas deferens (Figures 4, 5, and 9), we could not see significant height differences.

3.2 | Functional significance of the localization of AQP9, ENaC, and CFTR

All three channels we examined were localized on the apical border of the epithelia. However, only ENaC and AQP9, but not CFTR, showed a strong presence on the stereocilia (Figures 7–12). The localization of all three channels, on the apical surface of the columnar epithelial cells, provides clear evidence that these channels are involved concurrently in the regulation of fluid and electrolyte balance in the lumen of the vas deferens. ENaC allows the flow of Na^+ ions from the lumen into the cytoplasm. The osmotic gradient, thus, generated provides the driving force for the passive flow of water through AQP channels (Saint-Criq & Gray, 2017; Zhang et al., 2012; Figure 1).

CFTR and ENaC have significant roles in the regulation of airway surface liquid in the lungs with mutual influences (Chambers, Rollins, & Tarran, 2007; Rauh et al., 2017; Saint-Criq & Gray, 2017). The interdependence of CFTR and ENaC led to a hypothesis that there may be a direct interaction between these channels. However, we demonstrated that in multiciliated cells, ENaC is localized along the whole length of motile cilia. In contrast, CFTR is localized on the apical membrane but not on cilia (Enuka et al., 2012). These findings refuted the hypothesis of direct physical interaction for at least cells with motile cilia (Enuka et al., 2012).

The present findings extend our earlier observations on cilia to stereocilia that have a backbone of actin filaments. CFTR is located on the cell membrane but not on the stereocilial extensions of the apical membrane (Figure 9). CFTR secretes anions from the cell into the lumen and does not need to be on the apical extensions. In contrast, ENaC and AQP serve as channels from the lumen into the cell and their localization on the stereocilia allows their function in the lumen at a high density that is possible with the increased surface area provided by the stereocilia.

Previously, we had reported for the first time that in the female reproductive tract and the respiratory airways, ENaCs are uniformly distributed on the surface of motile cilia, the backbone of which is microtubules (Enuka et al., 2012). Thus, in analogy to our suggestion for ENaC function on motile cilia, we now suggest that ENaCs on stereocilia also serve as sensors for the regulation/absorption of electrolytes in the vas deferens lumen. A few previous studies have indicated that ENaC subunits may be linked directly to actin or actin-binding proteins (Mazzochi, Bubien, Smith, & Benos, 2006; Sasaki et al., 2014). Thus, the proximity of the ion channels to the actin filaments may have additional functional significance.

In addition to the luminal surface, smooth muscle layers covering the inner mucosa of vas deferens also showed strong ENaC, AQP9, and CFTR immunofluorescence. In Table 1, we summarized our results on the expression of ENaC and CFTR in the epithelia of the male reproductive system.

The expression of ENaC in smooth muscle cells has been shown in many organs including vascular smooth muscle (Drummond, Grifoni, & Jernigan, 2008; Kusche-Vihrog, Tarjus, Fels, & Jaisser, 2014), epididymis (Sharma & Hanukoglu, 2019), arrector pili muscle cells in skin (Hanukoglu et al., 2017), and renal microvascular smooth muscle cells (Guan, Pollock, Cook, Hobbs, & Inscho, 2009). It has been suggested that ENaC functions as a mechanosensor in vascular smooth muscle cells that initiate pressure-induced constriction known as the "myogenic response" (Drummond & Stec, 2015). Extending these earlier findings, we suggest that ENaC has a role in the function of vas deferens smooth muscle cells that remain to be defined.

TABLE 1 Expression of ion channels ENaC and CFTR in male reproductive organs

Organ	Tissue/cells	ENaC	CFTR	References
Testis	Sertoli cells	+	+	Sharma et al. (2018)
	Germ cells	+	–	
	Spermatozoa	+	ND	
	Peritubular myoid cells	–	–	
	Interstitial cells	–	–	
Epididymis	Initial segment	+	+	Sharma and Hanukoglu (2019)
	Caput epithelia	+	+	
	Corpus epithelia	+	+	
	Cauda epithelia	+	[a]	
	Smooth muscle myoid cells	+	+	
	Interstitial muscle tissue	+	+	
Vas deferens	Columnar epithelia	+	+	Present study
	Basal layer	+	–	
	Smooth muscle layers	+	+	

Abbreviations: CFTR, cystic fibrosis transmembrane conductance regulator; ENaC, epithelial sodium channel; ND, not determined
[a]Only in principal cells.

3.3 | Clinical implications of the findings

These findings raise questions about the routes and the mechanisms by which mutations in the CFTR gene lead to diverse genetic problems. Several groups who have examined large cohorts of patients with CFTR mutations have reported some genotype–phenotype relationships (de Souza et al., 2018; Yuan et al., 2019). Yet, the molecular mechanisms by which the CFTR mutations lead to problems of organogenesis remain ununderstood. In our recent study on the localization of CFTR in the testis, we reported CFTR immunofluorescence specifically in the nuclei of Sertoli cells. On the basis of these findings, we suggested that CFTR may have a direct effect on gene expression in addition to its function as an ion channel (Sharma et al., 2018).

In contrast to CFTR, mutations in ENaC subunit genes are associated with specific symptoms of multisystem PHA Type I and without problems of organogenesis (Hanukoglu & Hanukoglu, 2016). In a female patient with a nonsense mutation in ENaCα, we recently reported that ENaC is not expressed in the endometrial epithelia and that the mutation is associated with female infertility (Boggula et al., 2018). With the strong expression of ENaC along with the whole male reproductive system, it would be expected that ENaC mutations will have a deleterious effect also on male fertility. The few known male PHA patients have not reached yet marital status, and their fertility status remains unknown. The effect of ENaC mutations on the fertility of experimental animals is hard to study since the knock-out animals of ENaC α-subunit do not survive due to the defects in the perinatal lung liquid clearance (Bonny & Hummler, 2000).

The interdependence of the function of the three channels (ENaC, CFTR, and AQP9) raises the possibility that some cases of infertility may be dependent on the concurrent appearance of mutations in more than one of the genes coding for these channels.

4 | MATERIALS AND METHODS

4.1 | Antibodies and fluorescent tags

The rabbit polyclonal anti-ENaCα antisera against the extracellular domain of the α-subunit of human ENaC was generated in our lab and registered in the Antibody Registry (http://antibodyregistry.org/search?q=AB_2728747). The specificity of the anti-ENaCα antisera against the ENaCα subunit was determined by tagged protein expression in an Sf9 insect cell culture system and verified by mass-spectral analysis (Enuka et al., 2012). Other antibodies and fluorescent tags used in the study are listed in Table 2.

4.2 | Animals and tissue processing

Adult male Sprague–Dawley strain rats and Institute of Cancer Research mice, aged between 90 and 120 days, were housed according to the standard laboratory conditions with ad libitum access to food and water. The study protocol was approved by the Institutional Animal Ethics Committee of Ariel University (Ariel, Israel; permit 32_12733_b019), according to the Ministry of Health guidelines. The rat vas deferens were surgically removed immediately after CO_2 asphyxiation of each animal. For western blot, samples were snap-frozen in the liquid N_2. The mouse vas deferens was removed after cardiac perfusion. For immunofluorescence, the samples were kept in 4% paraformaldehyde in phosphate-buffered saline (PBS; 10 mM potassium phosphate, pH 7.4, and 150-mM NaCl) overnight. Samples were then transferred to 30% sucrose and kept at 4°C for at least 24 hr. Tissues were later embedded in optimal cutting temperature compound (Tissue-Tek, Sakura, The Netherlands) and stored at −80°C.

TABLE 2 Antibodies and fluorescent tags used in this study

Antibody/tag	Host, company, and catalog number	Application, dilution
Anti-ENaCα	Rabbit, Antibody Registry, #AB_2728747	IF-1:25, WB-1:1000
Anti-CFTR	Rabbit, Alomone Labs, #ACL-006	IF-1:25
Anti-AQP9	Rabbit, Alomone Labs, #AQP-009	IF-1:100
Alexa Fluor 555 IgG (H+L)	Goat anti-rabbit, Life Technologies, #A21428	IF-1:200
Peroxidase conjugate IgG (H+L)	Goat anti-rabbit, Jackson ImmunoResearch, #111-035003	WB-1:2000
CF488A conjugate phalloidin	Biotium, #BTM-00042	IF-1:20
DyLight™ 554 phalloidin	Cell Signaling Technology, #13054	IF-1:20

Abbreviations: AQP9, aquaporin-9; CFTR, cystic fibrosis transmembrane conductance regulator; ENaCα, epithelial Na^+ channel α-subunit; IgG, immunoglobulin G.

4.3 | Cryotomy and immunofluorescence staining

The tissue blocks were sliced to 30-μm-thick sections on a cryostat (Leica Jung 2000, Wetzlar, Germany) at −25°C and collected in PBS containing 0.1% sodium azide. For immunofluorescence labeling, tissues sections were permeabilized with 0.1% Tween-20 (Sigma-Aldrich) in PBS for 10 min and washed three times in PBS for 5 min each. The sections were then incubated in 300-μl 4% bovine serum albumin (BSA; Sigma-Aldrich) in PBS for 20 min, washed with PBS for 5 min, and incubated at 4°C either overnight with anti-ENaCα and anti-CFTR antisera or 18 hr with anti-AQP9 antisera in PBS containing 2% BSA. Sections were then washed six times in PBS (5 min each) and incubated with the secondary antiserum goat anti-rabbit immunoglobulin G (IgG) in PBS containing 2% BSA for 1 hr at room temperature. After six washes for 5 min each with PBS, nuclei were stained using the DAPI for 2 min.

Unless otherwise indicated, all the steps were carried out at room temperature. In control experiments, the same protocol was followed with the exception of primary antiserum that was either replaced by an antigen antibody complex (competitive experiment) or omitted from the reactions. In such control–antibody complex (competitive experiment) or omitted from the reactions. In such control slides, only the blue DAPI staining was visible. To stain the actin filaments, tissues slices were reacted with CF488A phalloidin conjugate (green) and DyLight™ 554 (red) phalloidin in PBS for 45 min at room temperature.

The sections were then transferred onto X-tra adhesive slides (Leica Biosystems, Peterborough, UK), mounted with antifade reagent glycerol containing n-propyl gallate (Sigma-Aldrich) in 100-mM phosphate buffer (pH 7.2). Experiments were performed at least three times with independent results.

4.4 | Confocal microscopy

High-resolution fluorescent images were acquired using an LSM 700 confocal microscope (Carl-Zeiss, Germany). The laser diodes used in the image acquisition were 405 nm for DAPI, 488 nm for CF488A, and 555 nm for Alexa Fluor 555 and DyLight™ 554. The fluorescence and bright-field illumination modes were used during the image acquisition process. Samples were visualized through LCI plan-apochromat ×25/0.8, EC plan-neofluar ×40/1.30 oil, and plan-apochrom at ×63/1.40 oil objective lenses. The composite images were generated using the tile-scan image overview mode. Three-dimensional images were generated by compiling images from z-stack optical sectioning of tissue sections.

4.5 | Protein gel electrophoresis and western blots

Western blot analyses were carried out as previously described (Sharma et al., 2018). Briefly, the frozen tissue samples from the lung, testis, epididymis, and vas deferens were homogenized in the lysis buffer (50 mM Tris-buffer [pH 7.4], 1 mM EDTA, and proteases inhibitors cocktail). The protein concentration was determined using the Bradford method with BSA as a standard. The samples were dissolved in Laemmli sample buffer (50 mM Tris-HCl pH 6.8, 2% sodium dodecyl sulfate, 0.2% bromophenol blue, 10% glycerol, and 5% β-mercaptoethanol) and loaded onto an 8.5% polyacrylamide gel. After electrophoresis, the proteins were transferred onto a nitrocellulose membrane (Bio-Rad) using a BioRad apparatus. Initially, the membrane was blocked using 1% skimmed milk in PBS for 45 min at room temperature. The membrane was then reacted with anti-ENaCα antisera for 3 hr at room temperature in PBS containing 2% BSA. Afterward, the membrane was washed four times in PBS-T (0.1% Tween-20 in PBS, 5 min each).

The membrane was then incubated with secondary antibody peroxidase-conjugated goat anti-rabbit IgG in a freshly prepared PBS containing 2% BSA for 90 min at room temperature. The membrane was washed four times with 0.1% PBS-T for 5 min each. The peroxidase-labeled membrane was developed using a chemiluminescence method with luminol. The membrane was soaked in 12 ml buffer containing 0.1 M Tris, pH 8.5, 2.5 mM luminol, 400 μm p-coumaric acid and 3 μl hydrogen peroxide. After 1 min, the membrane was dried on filter paper and visualized by Image Quant LAS, 4000 mini (GE).

ACKNOWLEDGMENTS

The authors would like to thank Prof. Aaron Hanukoglu (Tel Aviv University, Sackler School of Medicine) for useful discussions and for his critical evaluation of the paper. This study was partially supported by funds from the Ariel University.

CONFLICT OF INTERESTS

The authors declare that there are no conflict of interests.

ETHICS STATEMENT

The study protocol was approved by the Institutional Animal Ethics Committee of Ariel University (Ariel, Israel) (permit 32_12733_b019), according to the Ministry of Health guidelines.

ORCID

Sachin Sharma http://orcid.org/0000-0002-6776-1061
Girishkumar K. Kumaran http://orcid.org/0000-0003-3000-7978
Israel Hanukoglu http://orcid.org/0000-0003-3889-0320

REFERENCES

Acott, T., & Carr, D. (1984). Inhibition of bovine spermatozoa by caudal epididymal fluid: II. Interaction of pH and a quiescence factor. *Biology of Reproduction*, *30*, 926–935. https://doi.org/10.1095/biolreprod30.4.926

Althaus, M. (2013). ENaC inhibitors and airway re-hydration in cystic fibrosis: State of the art. *Curr Mol Pharmacol*, *6*, 3–12. https://doi.org/10.2174/1874467211205990025

Andonian, S., & Hermo, L. (1999). Principal cells of the vas deferens are involved in water transport and steroid synthesis in the adult rat. *Journal of Andrology*, *20*, 158–176. https://doi.org/10.1002/j.19394640.1999.tb02508.x

Andonian, S., Jarvi, K., Zini, A., & Hermo, L. (2002). Ultrastructural features of the vas deferens from patients undergoing vasectomy and vasectomy reversal. *Journal of Andrology*, *23*, 691–701. https://doi.org/10.1002/j.1939-4640.2002.tb02312.x

Bertog, M., Smith, D. J., Bielfeld-Ackermann, A., Bassett, J., Ferguson, D. J., Korbmacher, C., & Harris, A. (2000). Ovine male genital duct epithelial cells differentiate in vitro and express functional CFTR and ENaC. *American Journal of Physiology: Cell Physiology*, *278*, C885–C894. https://doi.org/10.1152/ajpcell.2000.278.5.C885

Boggula, V. R., Hanukoglu, I., Sagiv, R., Enuka, Y., & Hanukoglu, A. (2018). Expression of the epithelial sodium channel (ENaC) in the endometrium—Implications for fertility in a patient with pseudohypoaldosteronism. *Journal of Steroid Biochemistry and Molecular Biology*, *183*, 137–141. https://doi.org/10.1016/j.jsbmb.2018.06.007

Bonny, O., & Hummler, E. (2000). Dysfunction of epithelial sodium transport: From human to mouse. *Kidney International*, *57*, 1313–1318. https://doi.org/10.1046/j.1523-1755.2000.00968.x

Brown, J. W., & McKnight, C. J. (2010). Molecular model of the microvillar cytoskeleton and organization of the brush border. *PLoS One*, *5*, e9406. https://doi.org/10.1371/journal.pone.0009406

Cai, H., Qing, X., Niringiyumukiza, J. D., Zhan, X., Mo, D., Zhou, Y., & Shang, X. (2019). CFTR variants and renal abnormalities in males with congenital unilateral absence of the vas deferens (CUAVD): A systematic review and meta-analysis of observational studies. *Genetics in Medicine*, *21*, 826–836. https://doi.org/10.1038/s41436-018-0262-7

Canessa, C. M., Merillat, A. M., & Rossier, B. C. (1994). Membrane topology of the epithelial sodium channel in intact cells. *American Journal of Physiology*, *267*, C1682–C1690. https://doi.org/10.1152/ajpcell.1994.267.6.C1682

Carlin, R. W., Lee, J. H., Marcus, D. C., & Schultz, B. D. (2003). Adenosine stimulates anion secretion across cultured and native adult human vas deferens epithelia. *Biology of Reproduction*, *68*, 1027–1034. https://doi.org/10.1095/biolreprod.102.009381

Carlin, R. W., Sedlacek, R. L., Quesnell, R. R., Pierucci-Alves, F., Grieger, D. M., & Schultz, B. D. (2006). PVD9902, a porcine vas deferens epithelial cell line that exhibits neurotransmitter-stimulated anion secretion and expresses numerous HCO3(-) transporters. *American Journal of Physiology: Cell Physiology*, *290*, C1560–C1571. https://doi.org/10.1152/ajpcell.00468.2005

Carr, D. W., Usselman, M. C., & Acott, T. S. (1985). Effects of pH, lactate, and viscoelastic drag on sperm motility: A species comparison. *Biology of Reproduction*, *33*, 588–595. https://doi.org/10.1095/biolreprod33.3.588

Chambers, L. A., Rollins, B. M., & Tarran, R. (2007). Liquid movement across the surface epithelium of large airways. *Respiration Physiology & Neurobiology*, *159*, 256–270. https://doi.org/10.1016/j.resp.2007.06.005

Chen, H., Ruan, Y. C., Xu, W. M., Chen, J., & Chan, H. C. (2012). Regulation of male fertility by CFTR and implications in male infertility. *Human Reproduction Update*, *18*, 703–713. https://doi.org/10.1093/humupd/dms027

Cheung, K. H., Leung, C. T., Leung, G. P. H., & Wong, P. Y. D. (2003). Synergistic effects of cystic fibrosis transmembrane conductance regulator and aquaporin-9 in the rat epididymis1. *Biology of Reproduction*, *68*, 1505–1510. https://doi.org/10.1095/biolreprod.102.010017

Clausen, M. P., Colin-York, H., Schneider, F., Eggeling, C., & Fritzsche, M. (2017). Dissecting the actin cortex density and membrane-cortex distance in living cells by super-resolution microscopy. *Journal of Physics D: Applied Physics*, *50*, 064002. https://doi.org/10.1088/1361-6463/aa52a1

Clulow, J., Jones, R. C., & Hansen, L. A. (1994). Micropuncture and cannulation studies of fluid composition and transport in the ductuli efferentes testis of the rat: Comparisons with the homologous metanephric proximal tubule. *Experimental Physiology*, *79*, 915–928.

Clulow, J., Jones, R. C., Hansen, L. A., & Man, S. Y. (1998). Fluid and electrolyte reabsorption in the ductuli efferentes testis. *Journal of Reproduction and Fertility. Supplement*, *53*, 1–14.

Cooper, T. G., & Yeung, C. -H. (2003). Acquisition of volume regulatory response of sperm upon maturation in the epididymis and the role of the cytoplasmic droplet. *Microscopy Research and Technique*, *61*, 28–38. https://doi.org/10.1002/jemt.10314

Csanády, L., Vergani, P., & Gadsby, D. C. (2019). Structure, Gating, and Regulation of the CFTR Anion Channel. *Physiological Reviews*, *99*, 707–738. https://doi.org/10.1152/physrev.00007.2018

Dacheux, J. L., & Dacheux, F. (2014). New insights into epididymal function in relation to sperm maturation. *Reproduction*, *147*, R27–R42. https://doi.org/10.1530/REP-13-0420.

Da Silva, N., Piétrement, C., Brown, D., & Breton, S. (2006). Segmental and cellular expression of aquaporins in the male excurrent duct. *Biochimica Biophysica Acta*, *1758*, 1025–1033. https://doi.org/10.1016/j.bbamem.2006.06.026

Doctor, R. B. (2006). The Actin Cytoskeleton in the Apical Domain of Epithelial Cells. *Adv. Mol. Cell Biol. 37*, 25–47. https://doi.org/10.1016/S1569-2558(06)37002-6

Drummond, H. A., Grifoni, S. C., & Jernigan, N. L. (2008). A new trick for an old dogma: ENaC proteins as mechanotransducers in vascular smooth muscle. *Physiology (Bethesda, Md.)*, *23*, 23–31. https://doi.org/10.1152/physiol.00034.2007

Drummond, H. A., & Stec, D. E. (2015). βENaC acts as a mechanosensor in renal vascular smooth muscle cells that contributes to renal myogenic blood flow regulation, protection from renal injury and hypertension. *J. Nephrol. Res*, *1*, 1–9. https://doi.org/10.17554/j.issn.24100579.2015.01.12

Edelheit, O., Ben-Shahar, R., Dascal, N., Hanukoglu, A., & Hanukoglu, I. (2014). Conserved charged residues at the surface and interface of epithelial sodium channel subunits--roles in cell surface expression and the sodium self-inhibition response. *FEBS Journal*, *281*, 2097–2111. https://doi.org/10.1111/febs.12765

Edelheit, O., Hanukoglu, I., Shriki, Y., Tfilin, M., Dascal, N., Gillis, D., & Hanukoglu, A. (2010). Truncated beta epithelial sodium channel (ENaC) subunits responsible for multi-system pseudohypoaldosteronism support partial activity of ENaC. *Journal of Steroid Biochemistry and Molecular Biology*, *119*, 84–88. https://doi.org/10.1016/j.jsbmb.2010.01.002

Enuka, Y., Hanukoglu, I., Edelheit, O., Vaknine, H., & Hanukoglu, A. (2012). Epithelial sodium channels (ENaC) are uniformly distributed on motile cilia in the oviduct and the respiratory airways. *Histochemistry and Cell Biology*, *137*, 339–353. https://doi.org/10.1007/s00418-011-0904-1

Fettiplace, R., & Kim, K. X. (2014). The physiology of mechanoelectrical transduction channels in hearing. *Physiological Reviews*, *94*, 951–986. https://doi.org/10.1152/physrev.00038.2013

Francavilla, S., Moscardelli, S., Properzi, G., De Matteis, M. A., Scorza Barcellona, P., Natali, P. G., & De Martino, C. (1987). Postnatal development of epididymis and ductus deferens in the rat. A correlation between the ultrastructure of the epithelium and tubule wall, and the fluorescencemicroscopic distribution of actin, myosin, fibronectin, and basement membrane. *Cell and Tissue Research*, *249*, 257–265. https://doi.org/10.1007/bf00215508

Gentzsch, M., Dang, H., Dang, Y., Garcia-Caballero, A., Suchindran, H., Boucher, R. C., & Stutts, M. J. (2010). The cystic fibrosis transmembrane conductance regulator impedes proteolytic stimulation of the epithelial Na+ channel. *Journal of Biological Chemistry*, *285*, 32227–32232. https://doi.org/10.1074/jbc.M110.155259

Guan, Z., Pollock, J. S., Cook, A. K., Hobbs, J. L., & Inscho, E. W. (2009). Effect of epithelial sodium channel blockade on the myogenic response of rat juxtamedullary afferent arterioles. *Hypertension*, *54*, 1062–1069. https://doi.org/10.1161/HYPERTENSIONAHA.109.137992

Hamilton, D. W., & Cooper, T. G. (1978). Gross and histological variations along the length of the rat vas deferens. *Anatomical Record*, *190*, 795–809. https://doi.org/10.1002/ar.1091900403

Hanukoglu, I. (2017). ASIC and ENaC type sodium channels: Conformational states and the structures of the ion selectivity filters. *FEBS Journal*, *284*, 525–545. https://doi.org/10.1111/febs.13840

Hanukoglu, I., Boggula, V. R., Vaknine, H., Sharma, S., Kleyman, T., & Hanukoglu, A. (2017). Expression of epithelial sodium channel (ENaC) and CFTR in the human epidermis and epidermal appendages. *Histochemistry and Cell Biology*, *147*, 733–748. https://doi.org/10.1007/s00418-016-1535-3

Hanukoglu, A., Edelheit, O., Shriki, Y., Gizewska, M., Dascal, N., & Hanukoglu, I. (2008). Reninaldosterone response, urinary Na/K ratio and growth in pseudohypoaldosteronism patients with mutations in epithelial sodium channel (ENaC) subunit genes. *Journal of Steroid Biochemistry and Molecular Biology*, *111*, 268–274. https://doi.org/10.1016/j.jsbmb.2008.06.013

Hanukoglu, I., & Hanukoglu, A. (2016). Epithelial sodium channel (ENaC) family: Phylogeny, structurefunction, tissue distribution, and associated inherited diseases. *Gene*, *579*, 95–132. https://doi.org/10.1016/j.gene.2015.12.061

Hinton, B. T., & Palladino, M. A. (1995). Epididymal epithelium: Its contribution to the formation of a luminal fluid microenvironment. *Microscopy Research and Technique*, *30*, 67–81. https://doi.org/10.1002/jemt.1070300106

Höfer, D., & Drenckhahn, D. (1996). Cytoskeletal differences between stereocilia of the human sperm passageway and microvilli/stereocilia in other locations. *Anatomical Record*, *245*, 57–64. https://doi.org/10.1002/(SICI)1097-0185(199605)245:1<57::AID-AR10>3.0.CO;2-8

Hoffer, A. P. (1976). The Ultrastructure of the ductus deferens in man. *Biology of Reproduction*, *14*, 425–443. https://doi.org/10.1095/biolreprod14.4.425

Horisberger, J.-D. (2003). ENaC-CFTR interactions: The role of electrical coupling of ion fluxes explored in an epithelial cell model. *Pflugers Archiv: European Journal of Physiology*, *445*, 522–528. https://doi.org/10.1007/s00424002-0956-0

Howards, S. S., Jessee, S., & Johnson, A. (1975). Micropuncture and microanalytic studies of the effect of vasectomy on the rat testis and epididymis. *Fertility and Sterility*, *26*, 20–27. https://doi.org/10.1016/s00150282(16)40871-x

Hughey, R. P., Mueller, G. M., Bruns, J. B., Kinlough, C. L., Poland, P. A., Harkleroad, K. L., … Kleyman, T. R. (2003). Maturation of the epithelial Na+ channel involves proteolytic processing of the alpha- and gamma-subunits. *Journal of Biological Chemistry*, *278*, 37073–37082.

Jenkins, A. D., Lechene, C. P., & Howards, S. S. (1980). Concentrations of seven elements in the intraluminal fluids of the rat seminiferous tubules, rate testis, and epididymis. *Biology of Reproduction*, *23*, 981–987. https://doi.org/10.1095/biolreprod23.5.981

Jindal, S. K. (1984). Sperm concentration in different segments of the goat epididymis. *Theriogenology*, *22*, 545–551.

Johnson, A. L., & Howards, S. S. (1977). Hyperosmolality in intraluminal fluids from hamster testis and epididymis: A micropuncture study. *Science*, *195*, 492–493. https://doi.org/10.1126/science.835008

Jones, R. C. (1980). Luminal composition and maturation of spermatozoa in the genital ducts of the African elephant (*Loxodonta africana*). *Journal of Reproduction and Fertility*, *60*, 87–93.

Kennedy, S. W., & Heidger, P. M. (1979). Fine structural studies of the rat vas deferens. *The Anatomical Record*, *194*, 159–179. https://doi.org/10.1002/ar.1091940111

Khadijah Ramli, N. S., Giribabu, N., Karim, K., & Salleh, N. (2019). Hormonal control of vas deferens fluid volume and aquaporin expression in rats. *Journal of Molecular Histology*, *50*, 21–34. https://doi.org/10.1007/s10735-018-9804-1

Khadijah Ramli, N. S., Giribabu, N., & Salleh, N. (2018). Testosterone enhances expression and functional activity of epithelial sodium channel (ENaC), cystic fibrosis transmembrane regulator (CFTR) and sodium hydrogen exchanger (NHE) in vas deferens of sex-steroid deficient male rats. *Steroids*, *138*, 117–133. https://doi.org/10.1016/j.steroids.2018.06.012

Koslov, D. S., & Andersson, K.-E. (2013). Physiological and pharmacological aspects of the vas deferensan update. *Frontiers in Pharmacology*, *4*, 101. https://doi.org/10.3389/fphar.2013.00101

Kreda, S. M., & Gentzsch, M. (2011). Imaging CFTR protein localization in cultured cells and tissues. *Methods in Molecular Biology*, 15–33. https://doi.org/10.1007/978-1-61779-120-8_2

Kumaran, Girishkumar K., & Hanukoglu, Israel (2020). Identification and classification of epithelial cells in nephron segments by actin cytoskeleton patterns. *FEBS Journal*, https://doi.org/10.1111/febs.15088. in press.

Kusche-Vihrog, K., Tarjus, A., Fels, J., & Jaisser, F. (2014). The epithelial Na+ channel: A new player in the vasculature. *Current Opinion in Nephrology and Hypertension*, *23*, 143–148. https://doi.org/10.1097/01.mnh.0000441054.88962.2c

Levine, N., & Kelly, H. (1978). Measurement of pH in the rat epididymis in vivo. *Journal of Reproduction and Fertility*, *52*, 333–335. https://doi.org/10.1530/jrf.0.0520333

Levine, N., & Marsh, D. J. (1971). Micropuncture studies of the electrochemical aspects of fluid and electrolyte transport in individual seminiferous tubules, the epididymis and the vas deferens in rats. *Journal of Physiology*, *213*, 557–570. https://doi.org/10.1113/jphysiol.1971.sp009400

Mazzochi, C., Bubien, J. K., Smith, P. R., & Benos, D. J. (2006). The carboxyl terminus of the alphasubunit of the amiloride-sensitive epithelial sodium channel binds to F-actin. *Journal of Biological Chemistry*, *281*, 6528–6538. https://doi.org/10.1074/jbc.M509386200

Nagel, G., Barbry, P., Chabot, H., Brochiero, E., Hartung, K., & Grygorczyk, R. (2005). CFTR fails to inhibit the epithelial sodium channel ENaC expressed in *Xenopus laevis* oocytes. *Journal of Physiology*, *564*, 671–682. https://doi.org/10.1113/jphysiol.2004.079046

Osborne, L. R., Lynch, M., Middleton, P. G., Alton, E. W. F. W., Geddes, D. M., Pryor, J. P., … Santis, G. K. (1993). Nasal epithelial ion transport and genetic analysis of infertile men with congenital bilateral absence of the vas deferens. *Human Molecular Genetics*, *2*, 1605–1609. https://doi.org/10.1093/hmg/2.10.1605

Pastor-Soler, N., Bagnis, C., Sabolic, I., Tyszkowski, R., McKee, M., Van Hoek, A., … Brown, D. (2001). Aquaporin 9 expression along the male reproductive tract. *Biology of Reproduction*, *65*, 384–393. https://doi.org/10.1095/biolreprod65.2.384

Pelaseyed, T., & Bretscher, A. (2018). Regulation of actin-based apical structures on epithelial cells. *Journal of Cell Science*, *131*, jcs221853. https://doi.org/10.1242/jcs.221853

Phillips, M. L., & Schultz, B. D. (2002). Steroids modulate transepithelial resistance and Na+ absorption across cultured porcine vas deferens epithelia1. *Biology of Reproduction*, *66*, 1016–1023. https://doi.org/10.1095/biolreprod66.4.1016

Pierucci-Alves, F., Duncan, C. L., Lillich, J. D., & Schultz, B. D. (2010). Porcine vas deferens luminal pH is acutely increased by systemic xylazine administration. *Biology of Reproduction*, *82*, 132–135. https://doi.org/10.1095/biolreprod.109.078857

Rauh, R., Hoerner, C., & Korbmacher, C. (2017). δβγ-ENaC is inhibited by CFTR but stimulated by cAMP in *Xenopus laevis* oocytes. *Am. J. Physiol. Cell. Mol. Physiol. 312*, L277–L287. https://doi.org/10.1152/ajplung.00375.2016

Reynaert, I., Van Der Schueren, B., Degeest, G., Manin, M., Cuppens, H., Scholte, B., & Cassiman, J. -J. (2000). Morphological changes in the vas deferens and expression of the cystic fibrosis transmembrane

conductance regulator (CFTR) in control, ΔF508 and knock-outCFTR mice F508 and knock-outCFTR mice during postnatal life. *Molecular Reproduction and Development*, *55*, 125–135. https://doi.org/10.1002/(SICI)1098-2795(200002)55:2<125::AID-MRD1>3.0.CO;2-Q

Rodriguez, A., & Bustos-Obregón, E. (1993). Histophysiological and morphometric studies of the postnatal development of rat vas deferens. *Andrologia*, *25*, 29–37. https://doi.org/10.1111/j.1439-0272.1993.tb02678.x

Rojek, A. M., Skowronski, M. T., Fuchtbauer, E.-M., Fuchtbauer, A. C., Fenton, R. A., Agre, P., … Nielsen, S. (2007). Defective glycerol metabolism in aquaporin 9 (AQP9) knockout mice. *Proc. Natl. Acad. Sci. 104*, 3609–3614. https://doi.org/10.1073/pnas.0610894104

Saint-Criq, V., & Gray, M. A. (2017). Role of CFTR in epithelial physiology. *Cellular and Molecular Life Science*, *74*, 93–115. https://doi.org/10.1007/s00018-016-2391-y

Sasaki, S., Yui, N., & Noda, Y. (2014). Actin directly interacts with different membrane channel proteins and influences channel activities: AQP2 as a model. *Biochimica et Biophysica Acta/General Subjects*, *1838*, 514–520. https://doi.org/10.1016/j.bbamem.2013.06.004

Schimming, B., Pinheiro, P., de Matteis, R., Machado, C., & Domeniconi, R. (2015). Immunolocalization of Aquaporins 1 and 9 in the ram efferent ducts and epididymis. *Reproduction in Domestic Animals*, *50*, 617–624. https://doi.org/10.1111/rda.12537

Schlegel, P. N., Shin, D., & Goldstein, M. (1996). Urogenital anomalies in men with congenital absence of the vas deferens. *Journal of Urology*, *155*, 1644–1648. https://doi.org/10.1016/S0022-5347(01)66152-4

Sharma, S., & Hanukoglu, I. (2019). Mapping the sites of localization of epithelial sodium channel (ENaC) and CFTR in segments of the mammalian epididymis. *Journal of Molecular Histology*, *50*, 141–154. https://doi.org/10.1007/s10735-019-09813-3

Sharma, S., Hanukoglu, A., & Hanukoglu, I. (2018). Localization of epithelial sodium channel (ENaC) and CFTR in the germinal epithelium of the testis, sertoli cells, and spermatozoa. *Journal of Molecular Histology*, *49*, 195–208. https://doi.org/10.1007/s10735-018-9759-2

Snyder, P. M., McDonald, F. J., Stokes, J. B., & Welsh, M. J. (1994). Membrane topology of the amiloride-sensitive epithelial sodium channel. *Journal of Biological Chemistry*, *269*, 24379–24383.

de Souza, D. A. S., Faucz, F. R., Pereira-Ferrari, L., Sotomaior, V. S., & Raskin, S. (2018). Congenital bilateral absence of the vas deferens as an atypical form of cystic fibrosis: Reproductive implications and genetic counseling. *Andrology*, *6*, 127–135. https://doi.org/10.1111/andr.12450

Thomas, C. P., Auerbach, S., Stokes, J. B., & Volk, K. A. (1998). 5′ heterogeneity in epithelial sodium channel alpha-subunit mRNA leads to distinct NH2-terminal variant proteins. *American Journal of Physiology*, *274*, C1312–C1323.

Treuting, P. M., Dintzis, S. M., & Montine, K. S. (2017). *Comparative anatomy and histology: A mouse, rat and human atlas* (2nd ed.). Cambridge, MA: Academic Press.

Tuggle, K. L., Birket, S. E., Cui, X., Hong, J., Warren, J., Reid, L., … Fanucchi, M. V. (2014). Characterization of defects in ion transport and tissue development in cystic fibrosis transmembrane conductance regulator (CFTR) knockout rats. *PLoS One*, *9*(3), e91253. https://doi.org/10.1371/journal.pone.0091253

Wong, P. Y. D., Gong, X. D., Leung, G. P. H., & Cheuk, B. L. Y. (2002). Formation of the epididymal fluid microenvironment. In B. Robaire & B. T. Hinton (Eds.), *The epididymis: From molecules to clinical practice* (pp. 119–130). Boston, MA: Springer. https://doi.org/10.1007/978-1-46150679-9_7

Yeste, M., Morató, R., Rodríguez-Gil, J., Bonet, S., & Prieto-Martínez, N. (2017). Aquaporins in the male reproductive tract and sperm: Functional implications and cryobiology. *Reproduction in Domestic Animals*, *52*, 12–27. https://doi.org/10.1111/rda.13082

Yu, J., Chen, Z., Ni, Y., & Li, Z. (2012). CFTR mutations in men with congenital bilateral absence of the vas deferens (CBAVD): A systemic review and meta-analysis. *Human Reproduction*, *27*, 25–35. https://doi.org/10.1093/humrep/der377

Yuan, P., Liang, Z. K., Liang, H., Zheng, L. Y., Li, D., Li, J., … Wang, W. J. (2019). Expanding the phenotypic and genetic spectrum of Chinese patients with congenital absence of vas deferens bearing *CFTR* and *ADGRG2* alleles. *Andrology*, *7*, 329–340. https://doi.org/10.1111/andr.12592

Zhang, D., Tan, Y.-J., Qu, F., Sheng, J.-Z., & Huang, H.-F. (2012). Functions of water channels in male and female reproductive systems. *Molecular Aspects of Medicine*, *33*, 676–690. https://doi.org/10.1016/j.mam.2012.02.002

Zhou, W., De Iuliis, G. N., Dun, M. D., & Nixon, B. (2018). Characteristics of the epididymal luminal environment responsible for sperm maturation and storage. *Frontiers in Endocrinology*, *9*, 59. https://doi.org/10.3389/fendo.2018.00059

Zhou-Suckow, Z., Duerr, J., Hagner, M., Agrawal, R., & Mall, M. A. (2017). Airway mucus, inflammation and remodeling: Emerging links in the pathogenesis of chronic lung diseases. *Cell and Tissue Research*, *367*, 537–550. https://doi.org/10.1007/s00441-016-2562-z

How to cite this article: Sharma S, Kumaran GK, Hanukoglu I. High-resolution imaging of the actin cytoskeleton and epithelial sodium channel, CFTR, and aquaporin-9 localization in the vas deferens. *Mol Reprod Dev*. 2020;87:305–319. https://doi.org/10.1002/mrd.23317